Plankton lattices and the role of chaos in plankton patchiness

R. M. Hillary*
RRAG, Department of Environmental Science & Technology, Imperial College, London SW7 2BP, United Kingdom

M. A. Bees
Department of Mathematics, 15 University Gardens, University of Glasgow, Glasgow G12 8QW, United Kingdom
(Received 7 August 2003; published 31 March 2004)

Spatiotemporal and interspecies irregularities in planktonic populations have been widely observed. Much research into the drivers of such plankton patches has been initiated over the past few decades but only recently have the dynamics of the interacting patches themselves been considered. We take a coupled lattice approach to model continuous-in-time plankton patch dynamics, as opposed to the more common continuum type reaction-diffusion-advection model, because it potentially offers a broader scope of application and numerical study with relative ease. We show that nonsynchronous plankton patch dynamics (the discrete analog of spatiotemporal irregularity) arise quite naturally for patches whose underlying dynamics are chaotic. However, we also observe that for parameters in a neighborhood of the chaotic regime, smooth generalized synchronization of nonidentical patches is more readily supported which reduces the incidence of distinct patchiness. We demonstrate that simply associating the coupling strength with measurements of (effective) turbulent diffusivity results in a realistic critical length of the order of 100 km, above which one would expect to observe unsynchronized behavior. It is likely that this estimate of critical length may be reduced by a more exact interpretation of coupling in turbulent flows.

DOI: 10.1103/PhysRevE.69.031913 PACS number(s): 87.23.Cc, 05.45.Pq, 92.20.Rb

I. INTRODUCTION

The observation of patchiness in oceanic plankton populations is a well documented phenomenon [1]. Many driving mechanisms for patchiness have been suggested, from large scale turbulent advection [2] to small scale individual responses such as predator avoidance and buoyancy [3]. Regardless of the formative mechanism, the dynamics of these "patches" of plankton are generally not independent as many forms of coupling can exist between nearby patches (for instance, diffusive coupling or the effects of higher predatory choice). In this paper, we shall demonstrate that spatiotemporally varying dynamics can arise from a number of different sources. In Ref. [4] a "patchy" version of a standard reaction-diffusion equation was considered whereby each patch is diffusively coupled but has spatial variations in the reaction system. Specifically, these spatial variations were introduced to model the effect of fish school motion and spatial differences in higher predatory pressure. However, planktonic mixing behavior was modeled by an isotropic diffusion term so there was no investigation of any spatially heterogeneous mixing variations. Here, we propose a spatially one-dimensionally discretized paradigm for patch dynamics. Plankton populations are best represented as continuous time variables due to the effect of overlapping generations [5], so consider the following model:

$$\dot{\mathbf{S}}=\mathbf{F}(\mathbf{S})+(\mathcal{E}_L\otimes\mathcal{E}_S)\mathbf{S}, \tag{1}$$

where $\mathbf{S}=(\mathbf{s}_1,\mathbf{s}_2,\dots,\mathbf{s}_n)^T$ represents the species present (the $\mathbf{s}_i$ are m-dimensional vectors and $i=1,\dots,n$ denotes the lattice point). The reaction dynamics are governed by the function $\mathbf{F}(\mathbf{S})=[\mathbf{F}(\mathbf{s}_1),\mathbf{F}(\mathbf{s}_2),\dots,\mathbf{F}(\mathbf{s}_n)]^T$. The $n\times n$ lattice coupling matrix $\mathcal{E}_L$ is given by

$$\mathcal{E}_L=\begin{pmatrix} -\epsilon_2 & \epsilon_2 & 0 & \cdots & 0 \\ \epsilon_1 & -(\epsilon_1+\epsilon_3) & \epsilon_3 & \cdots & 0 \\ \vdots & \vdots & \vdots & \vdots & \vdots \\ 0 & \cdots & 0 & \epsilon_{n-1} & -\epsilon_{n-1} \end{pmatrix}, \tag{2}$$

and $\epsilon_i>0\ \forall\ i$. This defines a chain of n coupled oscillators with zero flux boundary conditions [6]. For our purposes, we consider the species coupling matrix $\mathcal{E}_S$ to be the m-dimensional identity matrix, meaning all species in each patch are locally coupled. For the case where $\epsilon_i=\epsilon\ \forall\ i$, it was seen in Refs. [7–9] that one can block diagonalize the Jacobian matrix for small perturbations of the globally synchronized state using discrete Fourier transforms which separate transverse variations (governing the stability of the synchronized regime) from variations inside the synchronized manifold. In general, there will be threshold values of the scalar coupling ϵ for which we see transitions from synchronized to unsynchronized dynamics. These values of ϵ are dependent upon the linearized reaction dynamics, the forms of the coupling matrices, $\mathcal{E}_L$ and $\mathcal{E}_S$, and also on the number of oscillators, n.

In the natural world, this symmetric form for the coupling is likely to be an overly optimistic assumption, leading us to consider the nonsymmetric coupling matrix seen in Eq. (2). We consider larger scale patchiness and, at these spatial scales, any movement between patches is most probably due to oceanic mixing (by and large not species dependent, hence the assumption that $\mathcal{E}_S=\mathbf{I}_m$) rather than individual motile responses.

*Email address: r.hillary@imperial.ac.uk

TABLE I. Default parameter values for the NPZ model defined in Eq. (3)

Parameter	Symbol	Default value
Phytoplankton growth rate	a	$0.2\ \mathrm{m}^{-1}\ \mathrm{day}^{-1}$
Light attenuation by water	b	$0.2\ \mathrm{m}^{-1}$
Light attenuation by phytoplankton	c	$0.4\ \mathrm{m}^2(\mathrm{g\,C})^{-1}$
Higher predation of zooplankton	d	$0.142\ \mathrm{g\,C\,m}^{-3}\ \mathrm{day}^{-1}$
Nutrient half-saturation constant	e	$0.03\ \mathrm{g\,C\,m}^{-3}$
Cross-thermocline exchange rate	k	$0.05\ \mathrm{day}^{-1}$
Phytoplankton respiration	r	$0.15\ \mathrm{day}^{-1}$
Phytoplankton sinking	s	$0.04\ \mathrm{day}^{-1}$
Lower mixed level nutrient concentration	N_0	$1\ \mathrm{g\,C\,m}^{-3}$
Zooplankton growth efficiency	α	0.25
Zooplankton excretion fraction	β	0.33
Regeneration of zooplankton excretion	γ	0.5
Zooplankton grazing rate	λ	$0.6\ \mathrm{day}^{-1}$
Zooplankton half-saturation constant	μ	$0.035\ \mathrm{g\,C\,m}^{-3}$
Patch to patch flux	ϵ_i	Bifurcation parameter

For individual dynamics that are chaotic, and where $\epsilon_i = \epsilon\ \forall\ i$, systems such as that in Eq. (1) are known to give rise to spatiotemporally chaotic dynamics, for certain regions of the coupling parameter space [6,9,10]. Also, for nonlocal coupling in the lattice, such systems display ''cluster'' synchronization [11,12]: certain patches are in synchronization, yet there is no synchronization between these synchronized clusters. In this paper we consider only simple diffusive, nearest-neighbor coupling, akin to a discretized reaction-diffusion system with no-flux boundary conditions.

To represent the reaction dynamics $\mathbf{F}$ we use a relatively simple three component nitrogen-phytoplankton-zooplankton (NPZ) biomass model, so that $\mathbf{s}=(N,P,Z)$. This particular NPZ model was constructed in Ref. [13] and investigated in detail in Refs. [14] and [15]. It takes the form

$$\frac{dN}{dt} = -\frac{Na}{(e+N)(b+cP)}P + rP + \frac{\lambda\beta P^2}{\mu^2+P^2}Z + \gamma dZ + k(N_0-N),$$

$$\frac{dP}{dt} = \frac{Na}{(e+N)(b+cP)}P - rP - \frac{\lambda P^2}{\mu^2+P^2}Z - (s+k)P,$$

$$\frac{dZ}{dt} = \frac{\alpha\lambda P^2}{\mu^2+P^2}Z - dZ. \tag{3}$$

Here, a is a measure of the maximum growth rate of P, b represents light attenuation by water, and c specific light attenuation by the phytoplankton themselves. The higher predation is denoted by d and e is the half-saturation constant due to the uptake of nutrient by the phytoplankton. Phytoplankton are lost from the system by two mechanisms, sinking of P given by s and the cross-thermocline exchange rate (with deep water devoid of phytoplankton) denoted by k. N_0 represents the nutrient level below the mixed layer and r the phytoplankton respiration rate. Here, α and β describe zooplankton growth efficiency and excretion. Finally, γ, λ, and μ denote the rates of recycled higher predation, zooplankton grazing, and the zooplankton grazing half-saturation coefficient, respectively. See Ref. [13] for more details. Typical parameter values and units of the above quantities are presented in Table I.

The nature of the higher predatory response is a somewhat contentious subject. The model as above employs a linear functional response, but it has been suggested that a quadratic or Holling type III form may be more appropriate. However, we choose the simple linear form so as not to entangle more complex higher predatory responses (including any density dependence which may possibly be associated with the predator having the option of choosing between prey patches) that may be better included in the patch coupling mechanism. The dynamics of the uncoupled system are well documented [15] from equilibria to stable limit cycles to chaos under variations of the closure (higher predation) rate d. Unless explicitly stated, we shall consider cases where the individual patch dynamics are chaotic as these cases are the most interesting in terms of possible routes to nonsynchronous patch dynamics. In the next two sections we show that, in our spatially discrete system, the transition to nonsynchronous collective dynamics can occur from a variety of different mechanisms. In Sec. II we introduce the concept of patch synchronization and describe numerical and theoretical results for the stability of our two patch paradigm system and how this might extend to an array of coupled patches, respectively. We also estimate a critical length for the transition from synchronous to nonsynchronous behavior, subject to a turbulent diffusive coupling assumption. In Sec. III we look at the effect of process noise and slight differences in the underlying patch reaction parameters. This latter phenomenon can lead to the generalized synchronization of the patches. Also, we discuss the role of chaotic dynamics in these phenomena and implications for plankton patch dynamics.

II. PATCH SYNCHRONIZATION

Our main aim is to reveal under what conditions the individual patch dynamics cease to be synchronous, giving rise to spatial (as well as temporal) irregularity throughout the patch lattice. Much work in recent years has been concerned with the general behavior and synchronization of coupled oscillators. By synchronization we mean that the asymptotic dynamics of all the individual patches are identical and are constrained to a manifold which we call $M_{\mathcal{S}}$ defined by

$$M_{\mathcal{S}}=\{\mathbf{s}_1,\mathbf{s}_2,\ldots,\mathbf{s}_n|\mathbf{s}_1(t)=\mathbf{s}_2(t)=\cdots=\mathbf{s}_n(t)\}. \tag{4}$$

By inspection of Eq. (2) we see that $\Sigma_j(\mathcal{E}_L)_{ij}=0$. Hence, the synchronization manifold $M_{\mathcal{S}}$ is invariant under the action of the flow defined in Eq. (1). The boundary of synchronous and nonsynchronous behavior corresponds to a symmetry breaking bifurcation by which the synchronous attractor $A\in M_{\mathcal{S}}$ loses stability transverse to $M_{\mathcal{S}}$. This "blowout" bifurcation [16,17] can be detected by calculating a variant of the Liapunov exponent. The Liapunov exponent [18] of the base point $x\in A$ in the direction $\mathbf{u}\in T_xM_{\mathcal{S}}$ is given by

$$\lambda(x,\mathbf{u})=\lim_{T\to\infty}\frac{1}{T}\int_0^T\ln\|DF^t(\mathbf{u})\|dt, \tag{5}$$

where DF^t represents the Jacobian of the dynamics at time t and $T_xM_{\mathcal{S}}$ is the tangent space of $M_{\mathcal{S}}$ at the point x. The *normal* Liapunov exponent, $\lambda_\perp(x,\mathbf{v})$, is defined as

$$\lambda_\perp(x,\mathbf{v})=\lim_{T\to\infty}\frac{1}{T}\int_0^T\ln\|\Pi_{(T_xM_{\mathcal{S}})^\perp}\circ DF^t(\mathbf{v})\|dt, \tag{6}$$

where $(T_xM_{\mathcal{S}})^\perp$ is the space normal to the tangent space $T_xM_{\mathcal{S}}$ and Π_V denotes an orthogonal projection onto the vector space V. If we assume that A supports some natural, ergodic invariant measure μ, then the time averages defined in Eq. (5) and Eq. (6) will be, almost everywhere, equal to the space averages

$$\lambda=\int_A\ln\|DF(\mathbf{u})\|d\mu(x) \tag{7}$$

and

$$\lambda_\perp=\int_A\ln\|\Pi_{(T_xM_{\mathcal{S}})^\perp}\circ DF(\mathbf{v})\|d\mu(x), \tag{8}$$

and consequently converge to a finite set of constant values referred to in Ref. [10] as the normal spectrum of the attractor A. These normal exponents measure the contraction or expansion of perturbations transverse to $M_{\mathcal{S}}$. If $\lambda_\perp^{\max}$ is the largest normal exponent then the sign of $\lambda_\perp^{\max}$ dictates the (local) stability of A. If it is negative then small perturbations will die out exponentially but if it is positive then disturbances initially grow $\sim e^{\lambda_\perp^{\max}t}$ until this growth is checked by the nonlinear terms (and A, while still an attractor in $M_{\mathcal{S}}$, has a basin of attraction with zero Lebesgue measure in the full phase space). Parameters such as the diffusive coupling ϵ are called *normal* parameters as they only affect the dynamics normal to $M_{\mathcal{S}}$. This ensures the continuity of the $\lambda_\perp$, with respect to normal parameters, allowing the definition of a clear bifurcation point. For normal parameters Ott and Sommerer [16] categorized the scenario into two types of behavior. After the loss of transverse stability, initial conditions close to A experience a transient orbit very similar to the chaotic trajectories in A. However, eventually they will move away toward some other attractor. The second case also has trajectories with nearby initial conditions shadowing orbits in A but they periodically burst away from synchronicity, a phenomenon known as *on-off intermittency*, only to return to the shadowing behavior. In the latter case, the nonsynchronous attracting set is said to be *stuck* [17] to the invariant manifold $M_{\mathcal{S}}$.

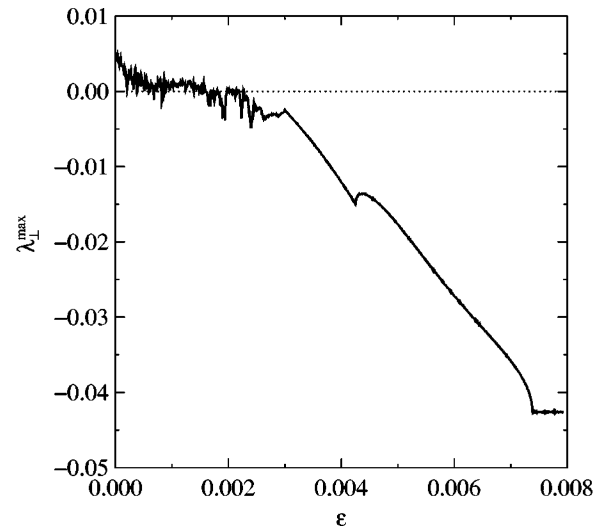

FIG. 1. A plot of the maximal normal Liapunov exponent $\lambda_\perp^{\max}$ vs the patch coupling ϵ. We see that the first blowout bifurcation occurs around $\epsilon_c=0.002$. Just below this value of the coupling, the synchronous state A will cease to be an attractor.

In Fig. 1 we present the maximal normal Liapunov exponent $\lambda_\perp^{\max}$, which has been calculated for the two patch, symmetric coupling case, $\epsilon_1=\epsilon_2=\epsilon$. We see that the synchronous state initially loses transverse stability below $\epsilon=\epsilon_c=0.002$ (3 d.p.) as $\lambda_\perp^{\max}$ passes through zero. There are isolated regions where the attractor regains transverse stability but, on the whole, the synchronized regime is unstable below this value of the coupling. In Fig. 2 we show the attractors in (N_1,N_2) space for $\epsilon_1=\epsilon_2=0.003$ (just above ϵ_c) and for $\epsilon_1=\epsilon_2=0.001$ (just below ϵ_c) to illustrate the form of solutions before and after the blowout bifurcation (this is an example of on-off intermittency).

The blowout bifurcation seen previously is not limited to a system of just two coupled oscillators. Transitions from globally synchronized to globally unsynchronized regimes have been seen [7–9], for a variety of different coupling matrices, $\mathcal{E}_L$ and $\mathcal{E}_S$, using various Rössler-type oscillators to represent $\mathbf{F}(\cdot)$. The asymmetric coupling scenario we consider is, we suggest, more biologically relevant but seems to have been hitherto largely ignored in the literature. The nonsymmetric nature of the lattice coupling matrix does not ad-

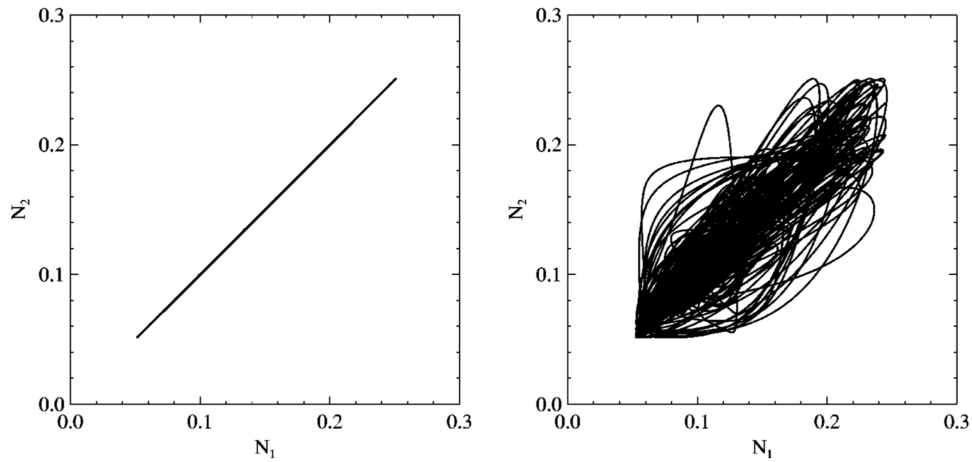

FIG. 2. Attractors in the (N_1,N_2) plane before, $\epsilon_1=\epsilon_2=0.003$ (left), and after, $\epsilon_1=\epsilon_2=0.001$ (right), the blowout bifurcation. We can clearly see that after the blowout bifurcation, the symmetry of the system is broken and N_1 and N_2 evolve in a nonsynchronous manner. We suggest in this paper that this is a possible route to plankton spatiotemporal patchiness.

mit by extension a spatially (discrete) modal decomposition and subsequent block diagonalization of the lattice Jacobian. For the symmetric case, this diagonalization allows for relative ease of numerical study of the transverse Liapunov exponents (corresponding to discrete spatial modes). Here, there appears to be no simple manner by which we can compute the transverse Liapunov exponents, thus making numerical study of such systems increasingly computationally expensive as n increases.

Of interest is the possibility that local coupling variations could also give rise to globally unsynchronized dynamics. To investigate this hypothetical scenario, let us consider the variational equation for the vector variable $\boldsymbol{\zeta}=(\boldsymbol{\zeta}_1,\ldots,\boldsymbol{\zeta}_{n-1})^T$, where $\boldsymbol{\zeta}_i=\mathbf{s}_i-\mathbf{s}_{i+1}$, with the Jacobian matrix DF evaluated at the synchronous solution ($\boldsymbol{\zeta}=\mathbf{0}$),

$$\dot{\boldsymbol{\zeta}}=(\mathbf{I}_{n-1}\otimes DF+\mathcal{E}_L^{\perp}\otimes\mathbf{I}_m)\boldsymbol{\zeta}, \tag{9}$$

and the $(n-1)\times(n-1)$ matrix $\mathcal{E}_L^{\perp}$ given by

$$\mathcal{E}_L^{\perp}=\begin{pmatrix} -(\epsilon_1+\epsilon_2) & \epsilon_3 & 0 & \cdots & 0 \\ \epsilon_1 & -(\epsilon_2+\epsilon_3) & \epsilon_4 & \cdots & 0 \\ 0 & \epsilon_2 & -(\epsilon_3+\epsilon_4) & \cdots & 0 \\ \vdots & \vdots & \vdots & \vdots & \vdots \\ 0 & \cdots & 0 & \epsilon_{n-2} & -(\epsilon_{n-1}+\epsilon_n) \end{pmatrix}. \tag{10}$$

The system in Eq. (9) is the variational equation for small perturbations transverse to the synchronization manifold. From the structure of $\mathcal{E}_L^{\perp}$, we can see that, barring the "boundary" lattice points $i=1$ and $n-1$, the coupling term ϵ_i directly affects only the dynamics of the variables $\boldsymbol{\zeta}_{i-1}$, $\boldsymbol{\zeta}_i$, and $\boldsymbol{\zeta}_{i+1}$. Let us consider the following decomposition of the full lattice phase space, S:

$$S=S_1\oplus S_2\oplus\cdots\oplus S_n, \tag{11}$$

and $\mathbf{s}_i\in S_i\ \forall\, i$. The variables $\boldsymbol{\zeta}_{i-1}$, $\boldsymbol{\zeta}_i$, and $\boldsymbol{\zeta}_{i+1}$ govern the fate of small perturbations of the synchronization manifold in the space $\mathcal{S}_i$, defined by

$$\mathcal{S}_i=\oplus_{j=i-1}^{i+2}S_j. \tag{12}$$

The simplest scenario that one could envisage is where, to begin with, $\epsilon_i=\epsilon\ \forall\, i$. We shall assume that there is some critical value of the scalar coupling, $\epsilon=\epsilon_c$ (depending on DF, $\mathcal{E}_L$, $\mathcal{E}_S$, and n), below which the synchronous state is unstable. If we have $\epsilon>\epsilon_c$, but $|\epsilon-\epsilon_c|\ll\epsilon_c$, then what happens to the system if just one of the lattice point coupling parameters, ϵ_i, is varied? Varying only this ϵ_i affects transverse perturbations of the synchronization manifold in the localized space $\mathcal{S}_i$. We expect that there exists a threshold value of ϵ_i for which small perturbations to the synchronization manifold in $\mathcal{S}_i$ do not die out and in fact grow, leading to the existence of one, positive normal Liapunov exponent. However, this locally originating blowout bifurcation must in fact manifest itself as a loss of stability of the globally synchronized state (a proof of which is given in Appendix A).

To illustrate this effect numerically, a lattice of eight diffusively coupled NPZ systems was considered. Numerical

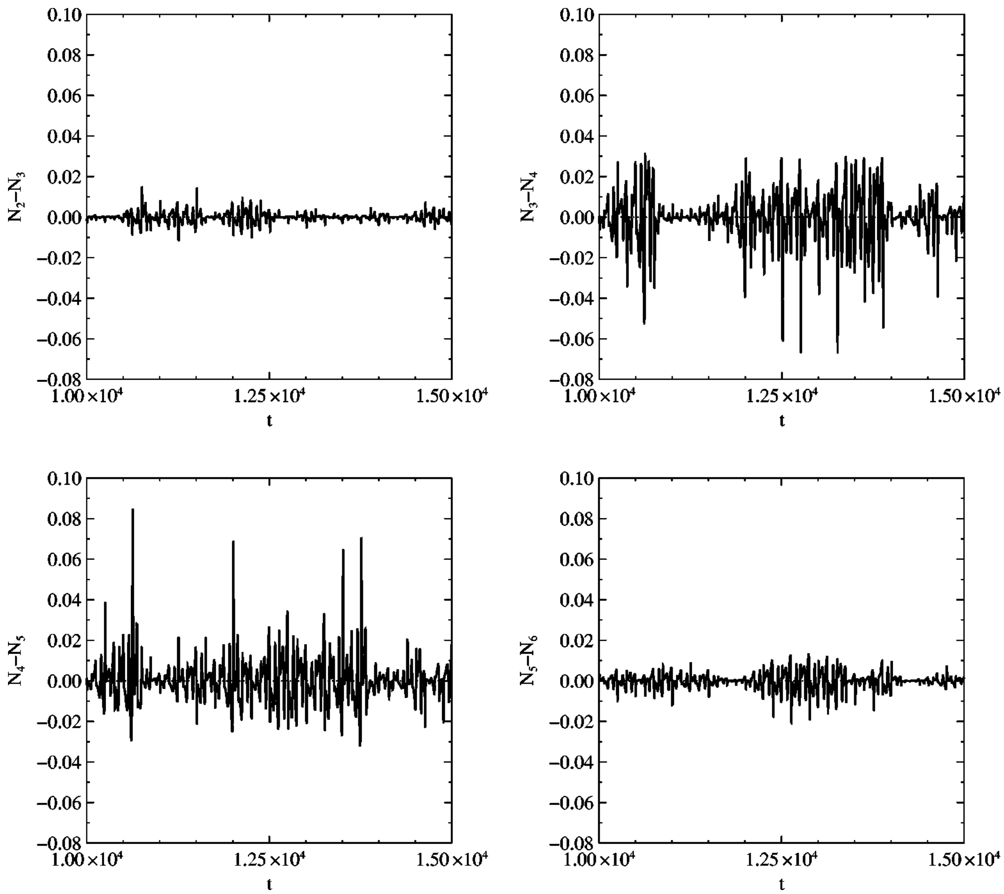

FIG. 3. $N_i(t)-N_{i+1}(t)$, for $i=2,3,4$, and 5 after any transient behavior has gone. The synchronized solution is unstable throughout the whole lattice. For this coupling scenario, $\epsilon_4=0.001$ and the other ϵ_i are set equal to 0.008, above the symmetric coupling threshold of $\epsilon\approx0.0075$. The simulations here were run for what amounts to many years, but the time scales of the nonsynchronous variations are on the scale of around a month or more. This is consisent with the large-scale temporal variations observed in plankton abundance.

investigation showed that, for the nearest-neighbor diffusive coupling with a single scalar ϵ to represent coupling strength, the eight patch system exhibited globally synchronous behavior for coupling strength above $\epsilon\approx0.0075$. In line with the theoretical scenario discussed previously, we reduced the value of one of the coupling parameters (in this case ϵ_4) when the system is close to the global loss of transverse stability. In Fig. 3, we plot the temporal difference in the nutrient variables for adjacent patches, N_i-N_{i+1}, for $i=2,3,4$, and 5 so that we look at the dynamics transverse to the synchronization manifold in the lattice points closest to the region where we have decreased the coupling. For ϵ_4 less than around 0.001, the globally synchronous state loses stability, giving rise to the dynamics seen in Fig. 3.

As can be seen from Fig. 3, the magnitude of the bursts from synchronicity are greatest in the two regions exactly adjacent to $i=4$. We quantify this bursting by computing the following time average:

$$\langle \zeta_i\rangle=\lim_{T\to\infty}\frac{1}{T}\int_0^T\|\zeta_i(t)\|dt=\lim_{T\to\infty}\frac{1}{T}\int_0^T\|\mathbf{s}_i(t)-\mathbf{s}_{i+1}(t)\|dt, \tag{13}$$

which (under the natural assumption that the attractor is ergodic) converges (almost everywhere) to a constant value, independent of the initial condition $(\zeta_1(0),\ldots,\zeta_{n-1}(0))$, for each i by Birkhoff's ergodic theorem (Eckmann and Ruelle [18]). Nonzero values of $\langle\zeta_i\rangle$ are indicative of nonsynchronous dynamics while for synchronized systems, $\langle\zeta_i\rangle$ will converge to zero as $T\to\infty$. Table II shows the numerical

TABLE II. Bursting measure defined in Eq. (13) for the case of a blowout from altering only one coupling parameter (row 1; $\epsilon_4=0.001$; $\forall\, i\neq4,\ \epsilon_i=0.008$) and where all the coupling parameters are equal but below the synchronization threshold (row 2; $\epsilon_i=0.001\ \forall\, i$).

i	1	2	3	4	5	6	7
$\langle\zeta_i\rangle$ ($\epsilon_4=0.001$; $\forall\, i\neq4,\ \epsilon_i=0.008$)	0.006	0.0045	0.012	0.013	0.0044	0.0037	0.0059
$\langle\zeta_i\rangle$ ($\epsilon_i=0.001\ \forall\, i$)	0.061	0.054	0.055	0.054	0.056	0.055	0.06

results for the values of the quantity defined in Eq. (13) for the situation where we lower only one value of the coupling (first row; $\epsilon_4 = 0.001$; $\forall\, i \neq 4$, $\epsilon_i = 0.008$) and when all the values of the coupling are the same but below the synchronization threshold (second row; $\epsilon_i = 0.001\, \forall\, i$).

As can be seen from Table II, for the first case we see that $\langle \zeta_i \rangle$ varies as we move away from the lattice point for which we decreased the coupling, yet it displays a symmetric decrease. This is in contrast with the second scenario where the corresponding lattice values of $\langle \zeta_i \rangle$ are almost identical. We point out that this similarity is not supported at the lattice boundary points. For periodic boundary conditions, the quantities $\langle \zeta_i \rangle$ converged to some value independent of i, for the symmetric coupling ($\epsilon_i = \epsilon\, \forall\, i$) case, due to the shift-invariant [7] nature of the coupling. Other statistics may reveal the nature of these effects.

It is worth noting that convergence of the bursting measures $\langle \zeta_i \rangle$ was quite slow, the results given were for 10^6 iterations; these differed little from results obtained at 750 000 iterations but did differ somewhat from results obtained at 500 000 iterations. We hypothesize that the reason for this is that the time average in Eq. (13) must be long enough to smooth out sporadic bursting effects.

These numerical simulations give some weight to the idea that, if we allow for local coupling variations, a global blowout can arise from a more localized event. As seen in Table II, the asynchronous bursting is strongest around the region where the coupling parameter is decreased. While computing the point at which the maximal normal Liapunov exponent becomes positive gives us the parameters for which synchronization becomes unstable, the simple ergodic average bursting quantity defined in Eq. (13) provides information on the local lattice dynamics after the blowout event, if only in terms of the severity of the asynchronous behavior.

A final, yet important, quantitative issue is whether these proposed blowout bifurcations, leading to plankton patchiness, are physically possible. In the system considered here, the coupling is of a spatially discrete, spatial-scale-dependent diffusive form; this may be considered a simplistic approach to modeling the turbulent transport of oceanic plankton. In the celebrated paper by Okubo [19], an experimental relationship between turbulent diffusion $D(\ell)$ and the spatial scale ℓ was derived for passive tracers in the horizontal plane. It was observed that, for $D(\ell)$ in $\mathrm{cm^2\,s^{-1}}$ and ℓ in cm,

$$D(\ell) \approx 0.01 \ell^{1.15}. \tag{14}$$

Given a specific number of patches, n say; a specified size ℓ of the patch system; and a corresponding spatial discretization and characteristic length scale, $\Delta = \ell/n$, the flux rate ϵ between adjacent patches satisfies $\epsilon(\Delta) \approx D(\Delta)/\Delta^2$. Thus, we can employ an empirical formula for ϵ, using Eq. (14), and

$$\epsilon(\Delta) \approx 0.01 n^2 \Delta^{-0.85}. \tag{15}$$

So, for $n=8$, if we let $\ell = 10^6$ cm (10 km), $\epsilon \approx 0.04\ \mathrm{day}^{-1}$; for $\ell = 10^7$ cm (100 km), we have that $\epsilon \approx 0.006\ \mathrm{day}^{-1}$; and for $\ell = 10^8$ cm (1000 km), $\epsilon \approx 0.0008\ \mathrm{day}^{-1}$. For our eight patch system, the critical coupling value, for the symmetric case, was $\epsilon \approx 0.0075$; this would then correspond to a length scale of around 100 km, for the number of patches described. This estimated relationship on the patch-to-patch flux (based on turbulent diffusive coupling) represents a kind of upper bound on the length scale (and number of patches) for which we expect to see synchronized patch dynamics. This is because the advective processes causing the coupling may manifest themselves at a length scale below Δ; as a result, the diffusive coupling strength would decrease, thus lowering the threshold for which unsynchronized patch dynamics are possible. The relationship in Eq. (15) suggests that both the extent of the patch system, ℓ, and the number of patches, n, strongly influence the realizable nature of the proposed blowout bifurcation to patchiness; for our particular model and coupling scenario, the above results suggest that such a blowout bifurcation can occur within a physically realistic, and experimentally observable, range of length scales.

For scenarios where more than one coupling parameter is varied, we can expect a more complicated interplay of local stabilizing and destabilizing influences. In general, when allowing for local coupling variations, one is almost certain to observe such locally originating blowout bifurcations, for a variety of coupling parameter combinations. We also hypothesize that, as was seen in the scalar coupling systems studied in Refs. [7–9], the nature of the coupling matrix, $\mathcal{E}_L$, and the number of coupled oscillators, n, will affect the occurrence of any loss of synchronization in the coupled lattice. Numerical simulations, for different numbers of patches, revealed similar behavior (but different critical values, as mentioned above) to that seen in our eight patch model system. Using other population models yields similar behavior; in fact, any system which exhibits blowout bifurcations in the well-studied symmetric coupling systems is very likely to display similar behavior to the examples given here. In these two senses (results qualitatively independent of the number of patches; behavior expected in any system displaying blowout behavior in the symmetric regime) we would consider the results robust, in terms of general coupled systems. Allowing asymmetric coupling entrains a richer variety of behavior and, although we have touched on some of the theoretical aspects of this type of coupling, more work is needed to fully elucidate the nature of the driving mechanisms.

III. FURTHER PATHWAYS TO IRREGULAR PATCH DYNAMICS

In the preceding section we described how sufficiently small levels of the coupling parameters allow for the onset of spatiotemporally heterogeneous patch dynamics via the loss of transverse stability of the synchronized state, but this is not the only desynchronizing mechanism. We have not yet addressed the situation where there are differences in the underlying reaction dynamics of each patch and we must also consider the effect of low levels of system noise.

Riddled basins of attraction were first investigated in Ref. [20]. A basin of attraction $\beta(A)$ of an invariant set A is said to be *locally riddled* if there exists $\delta > 0$ such that, for arbitrary $x \in \beta(A)$ and any $\varepsilon > 0$, the ε ball $B_\varepsilon(x)$ contains a positive measure set of points whose orbits exceed a distance δ from A. A basin of attraction is *globally riddled* if, for arbitrary $x \in \beta(A)$, $B_\varepsilon(x)$ intersects $\beta(A)$ and the basin of some other attractor with positive measure. This means that any open set in $\beta(A)$ will have a nonzero fraction that will either move a specified distance away from synchronicity (local riddling) or converge to another, nonsynchronous attractor (global riddling). If the basin of attraction of A, $\beta(A)$, is either locally or globally riddled then the synchronous state will not be stable to low levels of noise. Riddled basins form when one of the saddle cycles, from the usual cascade to chaos, embedded in A becomes a repelling cycle. This causes the creation of infinitely many repelling ''tongues'' foliating off of A. For the case of local riddling, it is not too difficult to see that any amount of noise will, with probability 1, push all orbits into one of these repelling regions. The orbit will then move some specified distance from synchronicity. This phenomenon has been dubbed *attractor bubbling* [21]. For the case of global riddling, we have a more extreme version of attractor bubbling as the orbit is alternately moved into the basins of attraction of the nonsynchronous and synchronous attractors. Whether the basin is locally or globally riddled, noise driven intermittency (attractor bubbling) will give similar patch dynamics to the postblowout scenario described previously.

Numerical investigations did not reveal the presence of riddling (either local or global) for this particular system. Global riddling has been observed in discrete, skew-product type population models [22] and local riddling seems a generic phenomenon in coupled oscillators so the absence of riddling here does not imply that it cannot occur for a different system. Intuitively, however, global riddling is not a likely phenomenon in such coupled systems. This is due to the strong nonlinear restraining mechanisms of most continuous population models (boundedness and positivity of solutions). This first property removes the basin boundary crisis route from locally to globally riddled basins [23] as this requires the (locally riddled) basin of the synchronous state to collide with its corresponding absorption area. For such population models as these, with bounded, positive solutions for all bounded, positive initial conditions, this scenario seems very unlikely. The only other route to a globally riddled basin is the emergence of a new, nonsynchronous attractor located in one of the repelling regions of the locally riddled basin of attraction. The biderectional, diffusive nature of the coupling (for positive values of the coupling matrices at least) makes this route unlikely as well.

The final scenario we consider incorporates small discrepancies in the parameters of the reaction dynamics governing each patch. This is a more general case of Eq. (1) but where we allow for the fact that the dynamics governing each patch will not always be the same and $\mathbf{F}(\mathbf{S}) = (\mathbf{F}_1(\mathbf{s}_1), \mathbf{F}_2(\mathbf{s}_2), \ldots, \mathbf{F}_n(\mathbf{s}_n))^T$. This type of patch parameter variation has been examined in the continuum sense [4,25] with regard to spatiotemporal planktonic dynamics. It was found that by having distinct regions with different higher predatory pressure complex, spatiotemporally chaotic oscillations were possible. In this paper, we make no mention of the form of the parametric perturbation (such as stochastic or deterministic); we do, however, define it, at least in terms of its magnitude, in Appendix B.

Variation in the underlying parameters of plankton dynamics has been hypothesized to be a driver of phytoplankton blooms such as red tides [26] and it is also feasible that there are some variations in parameters over large spatial scales. What does this imply for our coupled patch lattice model? In general, there are three classes of behavior for systems with detuned parameters and each depends on the size of the parameter mismatch and the strength of the coupling. Exact synchronization of the systems is no longer possible. However, Afraimovich *et al.* [24] suggested a less rigid definition of synchronization in which the dynamics of individual patches are related by some continuous (possibly smooth) mapping and are thus said to be in *generalized synchronization* (GS). Hence there are three possibilities for the dynamics of the patch lattice.

(1) For small parameter mismatch and sufficiently strong coupling there exists a diffeomorphism mapping the dynamics of one patch to another (A is known as *normally hyperbolic* [27]).

(2) For coupling strength below a certain value, differentiability (and possibly other properties) are lost, but there still exists a continuous relation between patches [30,29].

(3) Increasing the parameter mismatch (or equally decreasing the coupling) can mean this deterministic relation is lost, and the patches evolve in an uncorrelated manner.

The first possibility, normal hyperbolicity of the attractor A, can be numerically established, again using Liapunov exponents. The definition of normal hyperbolicity [27] requires that vectors transverse to $T_x M_{\mathcal{S}}$ experience contraction stronger than vectors inside $T_x M_{\mathcal{S}}$. If this condition is satisfied then, for small parameter mismatches, the subsequent invariant manifold will be diffeomorphic to $M_{\mathcal{S}}$. In terms of Liapunov exponents, this means that we require that for all $x \in A$, $\mathbf{v} \in T_x M_{\mathcal{S}}^{\perp}$ and $\mathbf{u} \in T_x M_{\mathcal{S}}$,

$$\lambda_{\perp}^{\max}(x,\mathbf{v}) < \lambda_A^{\min}(x,\mathbf{u}), \tag{16}$$

where $\lambda_{\perp}^{\max}$ is the maximal normal Liapunov exponent and $\lambda_A^{\min}$ is the smallest Liapunov exponent of A. However, as noted in Ref. [28], this is only a necessary condition not sufficient as we cannot calculate the minimal Liapunov exponent for all the saddle cycles embedded in A. Whether this set of zero measure can generically effect the smooth persistence of A is still an open question.

For the NPZ system in the chaotic regime, we find that $\lambda_A^{\min} = -0.096$. We can directly compute this value because the unstable manifolds of the saddle cycles embedded in A are contained in A [18]. Consequently, the Liapunov exponents associated with these cycles are all positive and, hence, the smallest exponent must then be that of the ergodic measure of the chaotic attractor. Figure 4 shows a neutral normal hyperbolicity curve, in (ϵ_1, ϵ_2) space, for the case of two coupled NPZ systems. We add that the calculation of this curve did not make use of Newton's method to find the zeroes of the function $G(\epsilon_1,\epsilon_2) = \lambda_{\perp}^{\max}(\epsilon_1,\epsilon_2) - \lambda_A^{\min}(\epsilon_1,\epsilon_2)$ due to computational constraints. Instead we used an *ad hoc*

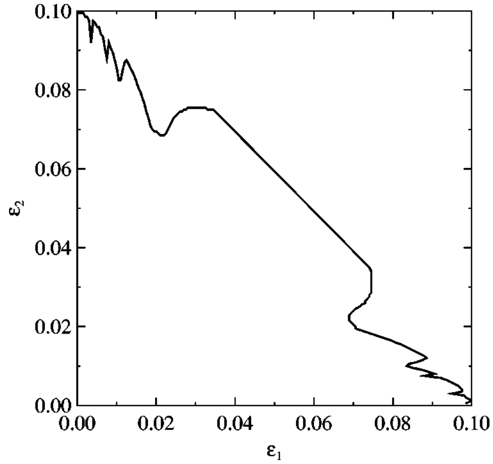

FIG. 4. A plot of the neutral normal hyperbolicity curve in (ϵ_1,ϵ_2) space. Above the curve the GS will be a diffeomorphism (up to a set of zero measure) but not below. Some of the symmetry of the curve is lost due to the *ad hoc* numerical procedure but the general trend is well captured.

search algorithm which we found captured much of the curve but unfortunately could not completely retain the curve's symmetry.

To look at how this property varies with the dynamics of the original patches Fig. 5 shows the same curve in (d,ϵ) space (symmetric coupling so $\epsilon=\epsilon_1=\epsilon_2$). Surprisingly we see that quite strong coupling is required for A to be normally hyperbolic, except within a neighborhood of the chaotic regime, $d=0.142$.

The existence of this effect is reinforced by consideration of Fig. 6 where we plot the Liapunov exponents of A with respect to the closure rate d. We find that there is always a relatively large negative exponent except around the chaotic regime. Very negative values of $\lambda_A^{\min}$ means we require strong coupling so that $\lambda_\perp^{\max}$ satisfies Eq. (16).

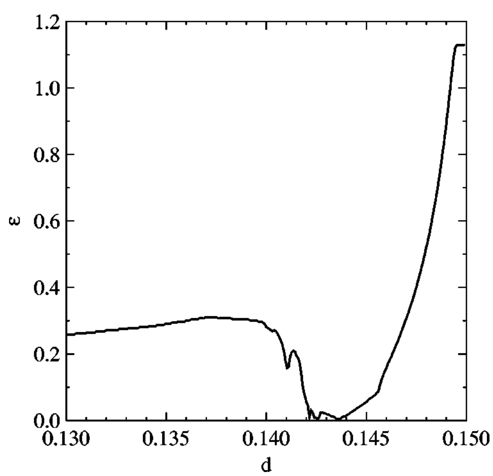

FIG. 5. Neutral normal hyperbolicity curve in (d,ϵ) space, over the same range as the plot of the Liapunov exponents of A in Fig. 6. Note that strong coupling is required for normal hyperbolicity except around the chaotic regime, something also seen in a similar figure calculated with a structurally different population model in Ref. [35].

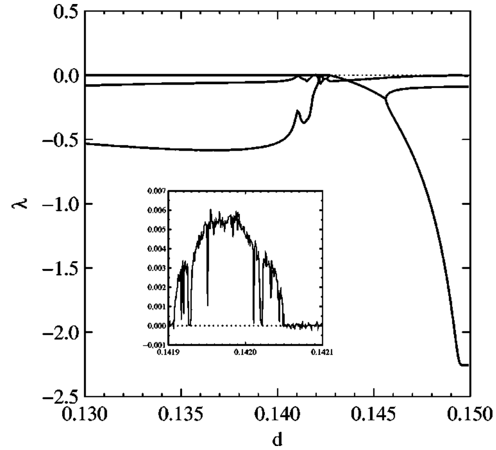

FIG. 6. Plot of the three Liapunov exponents of A as we vary the closure parameter d. The inset shows a close up round the chaotic region at $d\approx 0.142$. Note how the most negative Liapunov exponent is almost a (qualitative) mirror image of the neutral hyperbolicity curve in Fig. 5.

Here, and in other work on the generalized synchronization of detuned, normally hyperbolic identical oscillators [31], only two coupled oscillators were considered. The ideas presented by Josic [31] on normal k-hyperbolicity were for two coupled patches; in Appendix B we demonstrate how the invariant manifold ideas generalize to the smooth generalized synchronization of an arbitrary number of coupled, near-identical oscillators.

In coupled oscillator systems, such as the one we are considering, a very common type of generalized synchronization observed is *phase* synchronization, where the amplitudes of the oscillators vary in an unsynchronized manner, but the phases are identical. This has been observed in arrays of Rössler oscillators [32], in epidemiological models [33] and in three species resource-predator-prey models [34]. In another paper [35], we consider the implications of such phase synchronized dynamics in a more general ecological sense and the role that chaotic dynamics might have in the formation of smooth generalized synchronization.

IV. CONCLUDING REMARKS

By viewing interacting plankton patches as a form of coupled lattice model we have demonstrated several different routes by which transitions from synchronous (spatially homogeneous) to nonsynchronous (spatiotemporally varying) dynamical regimes may be observed. This noncontinuum approach allows us to classify some of these transitions in terms of bifurcations (blowout and riddling bifurcations). We use a two and an eight patch system as examples and describe how these results generalize to n coupled systems. Also we indicate what effect variations in patch system parameters may have and classify the types of generalized synchronization of patches. We also describe how one can compute areas of parameter space in which each definition applies.

We considered only normal coupling parameters here but it is likely that some system parameters will not be normal parameters. Similar transitions are observed when nonnormal parameters are varied (see the review in Ref. [36]).

In order to analyze field data one must be able to differentiate deterministic from stochastic relationships between patch dynamics and this requires further techniques. Tests for determinism exist; Ref. [29] developed a confidence statistic to measure properties of generalized synchronization and Ref. [30] used a variant on the idea of false nearest neighbors from time series as a test for determinism. In a paper currently in preparation we look at applying the idea of this weaker type of generalized synchronization to time series data of planktonic populations. Detecting deterministically evolving collective dynamics may allow one to average the individual dynamics in such a way (depending on the "strength" of generalized synchronization) as to minimize the error with the individual dynamics. These representative time series could then be used for the prediction of future trends and also as a more reliable data set for model fitting processes [5], as fitting often takes no account of the patchy nature of the sampled population.

Another open question concerns the existence of chaotic plankton dynamics. Due to the huge amount of effort required to collect a complete and reliable data set of spatiotemporal plankton distributions, it is difficult to distinguish between stochastic and possibly chaotic effects. However, field data of the dynamics of diatom communities in Ref. [37] showed good evidence for the presence of chaos. Our assumption of underlying chaotic dynamics allows for a natural transition to spatiotemporal (chaotic) variations (patchiness) in the plankton lattice dynamics. Using a model with equilibrium or limit cycle dynamics, in the spatially homogeneous case, requires certain sometimes *ad hoc* model augmentations (such as spatially distinct fish schools as seen in Refs. [25,4]) to see such observed complex dynamics when moving to a spatially extended model. Indeed, it has been suggested that chaos is a good natural state for populations, Ref. [38], in that chaotic fluctuations allow for the persistence of coexisting species and habitats, even in unfavorable conditions.

Using a simple argument based on the measured effective turbulent diffusivities of Okubo [19], we have shown, for our specific reaction model, that a blowout bifurcation to patchy dynamics is possible at a physically realistic scale of 100 km. However, it should be noted that this estimate is likely to be larger than estimates based upon better descriptions of mixing (and so coupling) in turbulent flows. Time scales of large scale patchiness show that spatiotemporal variations in the dynamics can occur over a time span of weeks and months [2,26]. These variations may be associated with bursting events from synchronicity (on similar time scales), as may be observed in Fig. 3. Continuum approaches to spatiotemporal plankton dynamics have usually included turbulent advection either by employing a simple, fixed-scale diffusive term [4,25] with spatial parameter variations, or some form of turbulent flow field [2,39]. In this paper, one view of our nonsymmetric coupling could be that of the turbulent (diffusive) transport of plankton, at some specified length scale. While these two approaches differ in their structure and methods, further work should concentrate on how these two viewpoints link together.

Initial numerical analyses of the case where the systems are no longer identical identified an area around the chaotic regime where the coupling strength needed to see smooth generalized synchronization of the patches was at its lowest. In Ref. [35], we investigate whether this is an isolated phenomenon as this could hint at an even more complex role for chaos in coupled population models.

From macro to micro scales, many ecosystems exhibit a patchy structure and factors such as migration mean that each population patch may be coupled to several of the others. With the added problems of irregular geometries and nonuniform coupling effects, it seems reasonable that a spatially discrete approach may sometimes be more appropriate and advantageous for the analysis of the dynamics.

ACKNOWLEDGMENT

The authors would like to acknowledge helpful discussions with and suggestions from P. Ashwin.

APPENDIX A: LOCALLY ORIGINATING GLOBAL BLOWOUT

To analytically demonstrate why a locally originating blowout bifurcation must manifest itself as a global loss of synchronization, we first assume that there is some value of $\epsilon_i > 0$ below which the maximal normal Liapunov exponent corresponding to the fate of small perturbations to the synchronization manifold in $\mathcal{S}_i$ [see Eq. (12)], $\lambda_\perp^{\max}(i)$, is positive.

By the multiplicative ergodic theorem of Oseledec [40], we can decompose the space orthogonal to the synchronization manifold, $TM_{\mathcal{S}}^\perp$, in the following manner. There exist linear subspaces $F_1 \supset \cdots \supset F_k$, such that $TM_{\mathcal{S}}^\perp = F_1 \oplus \cdots \oplus F_k$ [where $k = m(n-1)$], and

$$\lambda_\perp^j = \lim_{T\to\infty} \frac{1}{T}\int_0^T \ln \| \Pi_{TM^\perp} \bigcirc DG^t(\mathbf{v}) \| dt \quad \forall\, \mathbf{v} \in F_j \setminus F_{j+1}, \tag{A1}$$

where $\lambda_\perp^1 > \cdots > \lambda_\perp^k$, $\|\cdot\|$ is the Euclidean norm on $\mathbb{R}^{m(n-1)}$ and the $\lambda_\perp^j$ are the Liapunov exponents normal to $M_{\mathcal{S}}$. Next, we define the linear time evolution operator $\Lambda(t)$ for $\boldsymbol{\zeta}(t)$, which satisfies the following set of equations:

$$\boldsymbol{\zeta}(t) = \Lambda(t)\boldsymbol{\zeta}(0),$$

$$\frac{d\Lambda(t)}{dt} = \mathcal{J}^\perp \Lambda(t),$$

$$\Lambda(0) = \mathbf{I}_{m(n-1)}, \tag{A2}$$

where $\mathcal{J}^\perp$ is the bracket on the right hand side of Eq. (9). The normal Liapunov exponents can now be defined [7,18] to be the logarithms of the eigenvalues of the following limiting matrix:

$$\lim_{t\to\infty}[\Lambda^T(t)\Lambda(t)]^{1/2t}. \tag{A3}$$

Let $W_1, \ldots, W_k$ be the eigenspaces of the eigenvalues $\alpha_1, \ldots, \alpha_k$ of the limiting matrix defined in Eq. (A3). Now,

$$\begin{aligned} F_k &= W_k \\ F_{k-1} &= F_k \oplus W_{k-1}, \\ &\vdots \\ F_1 &= F_2 \oplus W_1. \end{aligned} \tag{A4}$$

Let us now consider some generic transverse perturbation vector $\mathbf{w} \in TM_{\mathcal{S}}^{\perp}$, where

$$\mathbf{w} = \mathbf{w}^1 + \mathbf{w}^2 + \cdots + \mathbf{w}^k \tag{A5}$$

and $\mathbf{w}^j \in W_j$. Since the matrix $\Lambda^T(t)\Lambda(t)$ is symmetric, the eigenvectors are orthogonal. Hence,

$$\|\mathbf{w}\|^2 = \sum_{j=1}^{k} \|\mathbf{w}^j\|^2, \tag{A6}$$

and furthermore, with $\mathbf{w}^T\Lambda^T(t)\Lambda(t)\mathbf{w} = \|\Lambda(t)\mathbf{w}\|^2$, we see that

$$\|\Lambda(t)\mathbf{w}\|^2 = \sum_{j=1}^{k} \|\Lambda(t)\mathbf{w}^j\|^2. \tag{A7}$$

Using the fact that $\lambda_{\perp}^{j} = \ln(\alpha_j)$,

$$\|\Lambda(t)\mathbf{w}\|^2 \approx e^{2\lambda_{\perp}^{1}t}\|\mathbf{w}^1\|^2 + \cdots + e^{2\lambda_{\perp}^{k}t}\|\mathbf{w}^k\|^2, \tag{A8}$$

and if we factor out the term in $e^{2\lambda_{\perp}^{1}t}$ we have that

$$\begin{aligned} \|\Lambda(t)\mathbf{w}\|^2 \approx e^{2\lambda_{\perp}^{1}t}(\|\mathbf{w}^1\|^2 + e^{2(\lambda_{\perp}^{2}-\lambda_{\perp}^{1})t}\|\mathbf{w}^2\|^2 + \cdots \\ + e^{2(\lambda_{\perp}^{k}-\lambda_{\perp}^{1})t}\|\mathbf{w}^k\|^2). \end{aligned} \tag{A9}$$

Now, as $t\to\infty$, $e^{2(\lambda_{\perp}^{j}-\lambda_{\perp}^{1})t} \to 0$ because $\lambda_{\perp}^{1} > \cdots > \lambda_{\perp}^{k}$. This means that the long term behavior of the perturbation $\mathbf{w}$ is dominated by the first term in Eq. (A8). However, we have one positive normal exponent and by definition this must be $\lambda_{\perp}^{1} = \lambda_{\perp}^{\max}(i)$. Hence, any generic perturbation will be exponentially expanded and we have a global blowout.

APPENDIX B: SMOOTH GENERALIZED SYNCHRONIZATION IN COUPLED OSCILLATOR ARRAYS

For the case of bidirectional coupling, as considered here, the paper by Josic [31] outlined the conditions needed to see smooth generalized synchronization in near-identical systems using invariant manifold theory. We now give a brief review of the essential results. Let us consider the following coupled dynamical system:

$$\begin{aligned} \dot{\mathbf{s}}_1 &= \mathbf{F}(\mathbf{s}_1) + \mathbf{G}_1(\mathbf{s}_1, \mathbf{s}_2), \\ \dot{\mathbf{s}}_2 &= \mathbf{F}(\mathbf{s}_2) + \mathbf{G}_2(\mathbf{s}_1, \mathbf{s}_2), \end{aligned} \tag{B1}$$

in $\mathbb{R}^{2m}$. Assuming that the m-dimensional synchronization manifold $M_{\mathcal{S}}$ is invariant and locally attracting, what happens after a small perturbation to the underlying dynamics, defined at least in magnitude by $\varepsilon \ll 1$.

For a suitably small perturbation, if the original invariant manifold (and the attracting state A therein) is normally k-hyperbolic (for some positive integer k), then the invariant manifold resulting from the perturbed dynamics, $M_{\mathcal{S}}^{\varepsilon}$, will be *diagonal-like* [31] and diffeomorphic [27] to $M_{\mathcal{S}}$. The notion of normal k-hyperbolicity is the same as that in Eq. (16), save that the contraction of vectors normal to the manifold must now be k times greater than that of vectors inside the tangent space of the manifold.

This means that, given the projections, Π^1 and Π^2, of orbits on the attractor A onto the phase spaces of the subsystems, $\mathbf{s}_1$ and $\mathbf{s}_2$, respectively, the diagonal-like nature of the perturbed manifold $M_{\mathcal{S}}^{\varepsilon}$ implies the existence of a diffeomorphism between the sets $\Pi^1(A^{\varepsilon})$ and $\Pi^2(A^{\varepsilon})$. So, we have the existence of some diffeomorphism φ such that $\mathbf{s}_2(t) = \varphi(\mathbf{s}_1(t))$, for orbits on the attractor *only*. In fact, the perturbed attractor A^{ε} can be expressed as the graph of the function $\varphi: \mathbb{R}^m \to \mathbb{R}^m$.

Now, we generalize these ideas to n-coupled oscillators by noticing that the identical synchronization manifold is again an m-dimensional submanifold of the full phase space in $\mathbb{R}^{mn}$. Suppose once again that there exists a locally attracting state $A \subset M_{\mathcal{S}}$. As before, if we can guarantee that the largest Liapunov exponent normal to $M_{\mathcal{S}}$ is smaller than the smallest Liapunov exponent inside of $M_{\mathcal{S}}$ (or k times smaller for normal k-hyperbolicity) then the synchronization manifold will persist, becoming $M_{\mathcal{S}}^{\varepsilon}$, which is diffeomorphic to $M_{\mathcal{S}}$. Once again, this means that, given the projections Π^i onto the phase space of the subsystem denoted by i, there exists a diffeomorphism φ_i between the sets $\Pi^i(A^{\varepsilon})$ and $\Pi^{i+1}(A^{\varepsilon})$, for $i = 1, \ldots, n-1$. Consequently, $\forall\, i \neq j$, the vector $\mathbf{s}_j(t)$ is (smoothly) expressible in terms of the vector $\mathbf{s}_i(t)$. We can also analogously express the generally synchronized attractor as the graph of the function $\Phi: \mathbb{R}^m \to \mathbb{R}^{m(n-1)}$ and

$$[\mathbf{s}_2(t), \mathbf{s}_3(t), \ldots, \mathbf{s}_n(t)] = \Phi(\mathbf{s}_1(t)), \tag{B2}$$

where

$$\Phi_i = \varphi_i \bigcirc \varphi_{i-1} \bigcirc \cdots \bigcirc \varphi_1. \tag{B3}$$

The generalization mentions nothing of the type of coupling in the oscillator array, save the caveat that the identical synchronization manifold be invariant under the (unperturbed) lattice dynamics.

[1] P.J.S. Franks, Limnol. Oceanogr. **5**, 1297 (1997).
[2] E.R. Abraham, Nature (London) **39**, 577 (1998).
[3] C.L. Folt and C.W. Burns, TREE **14**, 300 (1999).
[4] A.B. Medvinsky, I.A. Tikhonova, R.R. Aliev, B.-L. Li, Z.-S. Lin, and H. Malchow, Phys. Rev. E **64**, 021915 (2001).
[5] C. Jost and R. Arditi, Popul. Ecol. **43**, 229 (2001).
[6] C.W. Wu and L.O. Chua, IEEE Trans. Circuits Syst., I: Fundam. Theory Appl. **42**, 494 (1995).
[7] J.F. Heagy, T.L. Carroll, and L.M. Pecora, Phys. Rev. E **50**, 1874 (1994).
[8] L.M. Pecora and T.L. Carroll, Phys. Rev. Lett. **80**, 2109 (1998).
[9] L.M. Pecora, Phys. Rev. E **58**, 347 (1998).
[10] P. Ashwin, J. Buescu, and I. Stewart, Nonlinearity **9**, 703 (1996).
[11] K. Kaneko, Physica D **41**, 137 (1990); **54**, 5 (1991); **55**, 368 (1992); **75**, 55 (1994).
[12] V.N. Belykh, I.V. Belykh, and E. Mosekilde, Phys. Rev. E **63**, 036216 (2001).
[13] J.H. Steele and E.W. Henderson, J. Plankton Res. **14**, 157 (1992).
[14] A.M. Edwards and J. Brindley, Dyn. Stab. Syst. **11**, 347 (1996).
[15] A.M. Edwards and M.A. Bees, Chaos, Solitons Fractals **12**, 289 (2001).
[16] E. Ott and J.C. Sommerer, Phys. Lett. A **188**, 39 (1994).
[17] P. Ashwin, P. Aston, and M. Nicol, Physica D **111**, 81 (1998).
[18] J.-P. Eckmann and D. Ruelle, Rev. Mod. Phys. **57**, 617 (1985).
[19] A. Okubo, Deep-Sea Res. **18**, 789 (1971).
[20] J.C. Alexander, J.A. Yorke, Z. You, and I. Kan, Int. J. Bifurcation Chaos Appl. Sci. Eng. **2**, 795 (1992).
[21] P. Ashwin, J. Buescu, and I. Stewart, Phys. Lett. A **193**, 126 (1994).
[22] J.E. Franke and A.-A. Yakubu, Nonlinear Anal. Theory, Methods Appl. **16**, 111 (1991).
[23] T. Kapitaniak, Y. Maistrenko, A. Stefanski, and J. Brindley, Phys. Rev. E **57**, 6253 (1998).
[24] V.S. Afraimovich, N.N. Verichev, and M.I. Rabinovich, Inv. VUZ. Rasiofiz. RPQAEC **29**, 795 (1986).
[25] H. Malchow, B. Radtke, M. Kallache, A.B. Medvinsky, D.A. Tikhonov, and V.I. Petrovskii, Nonlinear Anal.: Real World Appl. **1**, 53 (2000).
[26] L. Legendre, J. Plankton Res. **12**, 681 (1990).
[27] S. Wiggins, *Normally Hyperbolic Invariant Manifolds in Dynamical Systems* (Springer-Verlag, New York, 1994).
[28] L. Kocarev, U. Parlitz, and R. Brown, Phys. Rev. E **61**, 3716 (2000).
[29] L.M. Pecora, T.L. Carroll, and J.F. Heagy, Phys. Rev. E **52**, 3420 (1995).
[30] N.F. Rulkov *et al.*, Phys. Rev. E **51**, 980 (1995).
[31] K. Josic, Phys. Rev. Lett. **80**, 3053 (1998).
[32] A.S. Pikovksy and M.G. Rosenblum, Physica D **104**, 219 (1997).
[33] D.J.D. Earn, P. Rohani, and B.T. Grenfell, Proc. R. Soc. London, Ser. B **265**, 7 (1998).
[34] B. Blasius and L. Stone, Int. J. Bifurcation Chaos Appl. Sci. Eng. **10**, 2361 (2000).
[35] R. M Hillary and M. A. Bees, Bull. Math Biol. (to be published).
[36] P. Ashwin, E. Covas, and R. Tavakol, Nonlinearity **12**, 563 (1998).
[37] G. Sughihara and R.M. May, Nature (London) **344**, 734 (1990).
[38] J. Allen, W. Schaffer, and D. Rosko, Nature (London) **364**, 229 (1993).
[39] R. Reigada, R.M. Hillary, M.A. Bees, J.M. Sancho, and F. Sagués, Proc. R. Soc. London, Ser. B **270**, 875 (2003).
[40] V.I. Oseledec, Trans. Mosc. Math. Soc. **19**, 197 (1968).